Mapping attenuation beneath North America using waveform cross-correlation and cluster analysis

Jesse F. Lawrence,[1] Peter M. Shearer,[1] and Guy Masters[1]

Received 19 January 2006; revised 22 February 2006; accepted 2 March 2006; published 13 April 2006.

[1] We measure seismic attenuation beneath North America using waveform cross-correlation and cluster analysis, and obtain images of the laterally varying anelastic structure of the upper mantle. Cluster analysis improves attenuation measurements by systematically comparing only highly similar waveforms, which reduces bias from scattering, directional differences in source functions, and source-side structure. While lacking station coverage in many areas, the *P*- and *S*-wave results are correlated ($R^2 \geq 0.5$) in both travel time and attenuation. Much weaker correlations are observed between travel-time and attenuation measurements. Similarities and differences between attenuation and travel times may be used to infer the source of the observed anomalies. The observed anelastic structure has a long-wavelength pattern crudely similar to that of seismic velocity, which likely indicates higher temperatures beneath western North America than in the east. Shorter-wavelength structure suggests complex variations requiring alternate explanations such as variable water content. **Citation:** Lawrence, J. F., P. M. Shearer, and G. Masters (2006), Mapping attenuation beneath North America using waveform cross-correlation and cluster analysis, *Geophys. Res. Lett.*, *33*, L07315, doi:10.1029/2006GL025813.

1. Introduction

[2] In recent years, great advances in North American geology have resulted from improved seismic tomography [e.g., *van der Lee and Nolet*, 1997; *Humphreys et al.*, 2003a]. Tomography has imaged the boundary between the tectonically active west (seismically slow) and the stable east (seismically fast). Elevated mantle temperatures beneath western North America [e.g., *Goes and van der Lee*, 2002] are inferred from elevated surface heat flow [*Morgan and Gosnold*, 1989], high elevation [*Kaben and Mooney*, 2001], thin crust [*Mooney et al.*, 1998], and negative long-wavelength Bouguer gravity anomalies [*Kane and Godson*, 1989]. While eastern North America has not undergone tectonic deformation since the Appalachian orogeny (350–450 Ma), western North America experienced several deformational episodes, which include the Laramide orogeny (35–75 Ma), the Basin and Range extension (~40 Ma), ongoing strike-slip faulting in California, and continued subduction beneath the northwest.

[3] This paper images lateral variations in anelastic and elastic structure beneath North America using a new, semi-automated technique called waveform cluster analysis [*Reif et al.*, 2002]. While tomographic imaging of elastic structure continues to gain higher resolution with increasing seismic data, the anelastic structure has trailed far behind. Seismic attenuation, or energy loss per cycle of a wave, is the standard seismic measure of anelasticity within the Earth. High attenuation beneath the tectonically active western North America [e.g., *Der and Lees*, 1985; *Lay and Helmberger*, 1983; *Lay and Wallace*, 1988] may result from hot upper-mantle temperatures compared to the cooler, more stable east. Yet, low velocity and high attenuation are not always correlated; the northwest is generally seismically slow and has low attenuation [*Lay and Wallace*, 1988], requiring an explanation other than thermal variations.

[4] Measuring attenuation is more difficult than measuring travel times because attenuation relies on the amplitude and frequency content of seismic waves, which are subject to contamination from source effects, focusing, multipathing, and scattering. Thus, attenuation studies lag behind velocity tomography studies in both resolution and repeatability of results. New and improved attenuation measurement techniques can greatly reduce the bias inherent in attenuation analysis. The most stable measure of attenuation beneath seismic stations is to compare one waveform with all other waveforms from the same event recorded at nearby stations and invert for a single differential attenuation measurement [e.g., *Venkataraman et al.*, 2004]. Yet without time-consuming quality control, this method is subject to the same contaminations. We present and implement a fast and efficient waveform cluster analysis method of attenuation measurement and produce maps of laterally varying attenuation beneath North America. We compare the attenuation with the travel times and draw some inferences about mantle structure.

2. Method

[5] Attenuation is often parameterized as t^*, the integrated sum of dt/Q along the ray path, where Q is quality factor. As with travel-time analysis [e.g., *VanDecar and Crosson*, 1990], measuring the relative attenuation of waveforms recorded at nearby stations for the same event reduces bias [e.g., *Flanagan and Wiens*, 1994; *Venkataraman et al.*, 2004]. These relative measures only reduce bias to the extent that the waveforms are similar; in general similarity decreases with increased station separation. Long-period teleseismic waves from the same event often correlate well among global seismic stations [*Reif et al.*, 2002]. However, directivity and source-side effects can cause significant waveform differences, which are problematic and time consuming for attenuation studies. Useful results can still be obtained quickly for subsets of the data using the cluster analysis method described below.

[1]Institute of Geophysics and Planetary Physics, Scripps Institution of Oceanography, La Jolla, California, USA.

0094-8276/06/2006GL025813$05.00

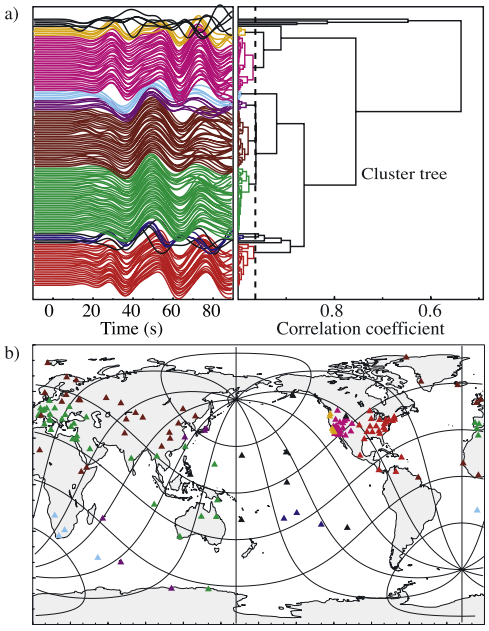

Figure 1. (a) Long-period *P*-wave records from 151 global seismic stations of a 1997 earthquake in the Kuriles grouped and aligned using waveform cluster analysis with a correlation cutoff of 0.965 (dashed line). The cluster "tree" is plotted on the right, showing correlation coefficients among different branches. Clusters with only one member are plotted in black. (b) Station locations correspond to the waveforms.

[6] We correct for instrument response and pre-filter the data between 0.01 and 0.1 Hz, rotate the horizontal components into the tangential direction, align the traces using the theoretical arrival times of the desired phases, and digitally display the results. The user then picks a time window for cross-correlation. We compute cross-correlation functions for every trace with every other trace using a time domain method that achieves sub-sample accuracy. We identify peaks in the cross-correlation function (positive and negative) that contain the differential time and scaling information. Using cluster analysis [e.g., *Hartigan*, 1975], the stations are sorted by waveform similarity and a cluster tree is plotted that shows at what level of correlation the groups may be joined (Figure 1). The user selects a minimum correlation coefficient cutoff for the division of waveforms into separate clusters. Different waveform clusters are indicated with different colors, which correspond to the station map shown beneath. Note that the clusters form spatially coherent groups of stations, reflecting radiation pattern and directivity differences from the source and/or propagation path. Consequently, stations divide into different clusters for different events. Choosing a higher cutoff results in a large number of clusters with fewer highly similar waveforms, which produces more accurate relative times, but having greater potential bias for each whole cluster.

[7] Optimal time shifts for the stations within each cluster are obtained using a weighted least squares method that also returns error estimates based on the internal consistency of the time shifts. The method permits polarity reversals in the waveforms by first solving for a best-fit set of polarities and then solving for the optimal time shifts. Results for both *P*- and *S*-wave analyses, indicate that our time measurements are more accurate than previous, single record time picks, and can be applied to more data in much less time [*Reif et al.*, 2002].

[8] Extending the method to measure attenuation is straightforward. We compute a differential t^* operator between every waveform pair in each cluster. This is measured from the slope of the spectral transfer function between the two waves [e.g., *Flanagan and Wiens*, 1994] assuming that quality factor is frequency independent between 0.08 and 0.083 Hz. These values are corrected with the theoretical attenuation difference calculated by tracing the ray paths through the 1D attenuation model, QL6 [*Durek and Ekstrom*, 1996]. Typically this correction is small because clusters tend to group records with small station separation. We only analyze records at stations between 45° and 85° from the event to further reduce the size of this correction and eliminate waves that may be affected by bottoming near the core-mantle boundary. We reconcile all of the differential t^* residuals into a single set of optimal relative t^* values for each station using the same least squares method mentioned above, which provides error estimates. An advantage of this approach is that the cross-correlation alignment ensures that we window exactly the same part of each waveform in computing t^*. Because we solve for both travel-time and attenuation, it is easy to test for correlations between these values. Once the cluster analysis is complete for all events, we solve for the attenuation and travel-time corrections for each cluster that minimize the scatter in the observations at each station. Because the station distributions for the clusters overlap, this removes the ambiguity arising from the relative measurements within individual clusters.

3. Results

[9] Figure 2 shows results of the method as applied to *P*- and *S*-wave arrivals from 112 earthquakes recorded by broadband stations in North America from 1995 to 2003. The cluster analysis was conducted using all GSN and temporary 1 Hz sampled data available at the IRIS DMS. We interpolate 2D curves between the median crust-corrected (CRUST2.0 [*Bassin et al.*, 2000]) measurements of each station as approximated by continuous curve splines under tension [*Smith and Wessel*, 1990]. Good azimuthal coverage ensures that the median measurement isolates the average velocity and attenuation structure beneath each station, reducing bias due to anomalies elsewhere along the ray path (see auxiliary material[1]). Ray path similarity and low heterogeneity in the lower mantle also reduce the bias of source-side and lower mantle effects. Interpolation provides more even coverage for easier comparison with heat flow and topography data.

[10] While the *S*-wave anomalies are generally larger amplitude than the *P*-wave anomalies, the *S*- and *P*-wave anomalies are similar. The *P*- and *S*-wave travel-time residuals are correlated at $R^2 = 0.5$ and the attenuation residuals

[1]Auxiliary material is available at ftp://ftp.agu.org/apend/gl/2006gl025813.

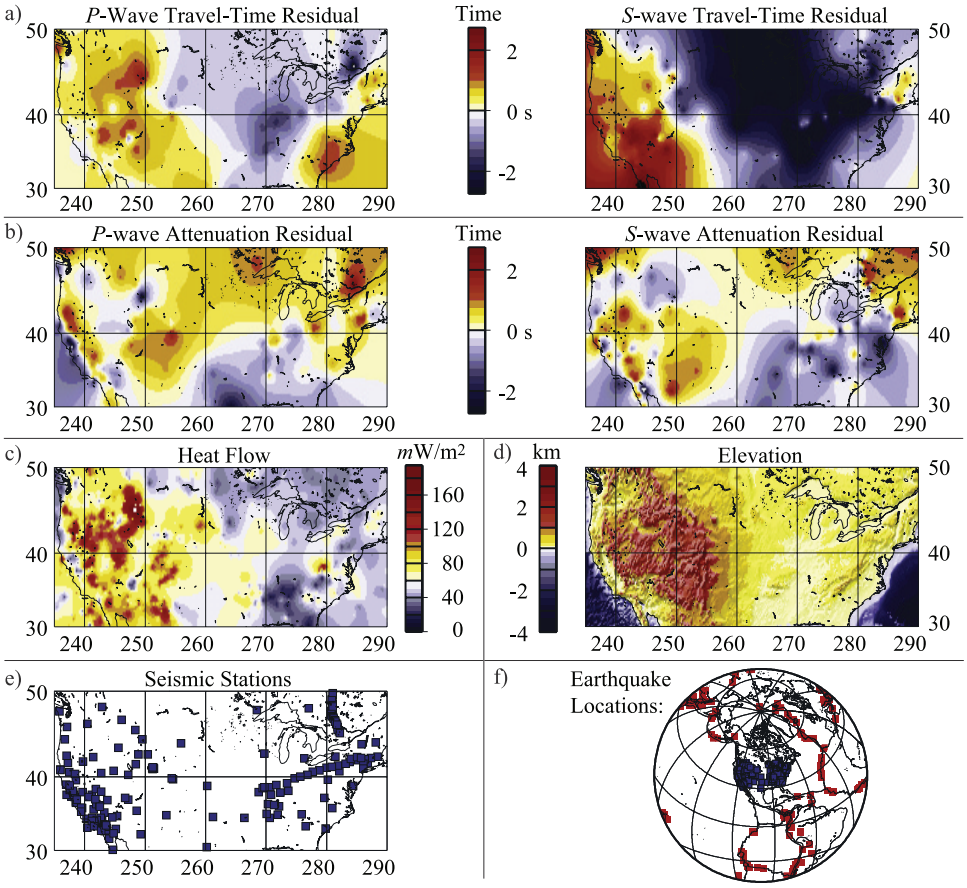

Figure 2. (a) *P*- and *S*-wave travel-time anomalies, (b) *P*- and *S*-wave attenuation anomalies, (c) compiled surface heat flow [*Pollack et al.*, 1993], and (d) topography [*Smith and Sandwell*, 1997]. The travel-time and attenuation residuals are smoothed and interpolated between the median values for each of (e) 216 stations (blue) which recorded at a total of (f) 112 earthquakes (red).

are correlated at $R^2 = 0.6$. Correlation between travel time and attenuation is low ($R^2 < 0.3$) for both *P*- and *S*-results. The western United States has slow *P*- and *S*-wave velocities compared to the east, with the dividing line occurring roughly along the eastern edge of the Rocky Mountains. These results are similar to those obtained in previous studies [e.g., *van der Lee and Nolet*, 1997]. Shear attenuation is strongest in New Mexico and the Basin and Range, consistent with results of *Patton and Taylor* [1984] and *Lay and Wallace* [1988], and is roughly correlated with heat flow measurements [*Pollack et al.*, 1993]. Seismic travel times and attenuation are crudely correlated, but there are interesting exceptions in some regions. For example, the Pacific Northwest has slow *S*-wave arrivals but normal to low attenuation, as previously noted by *Lay and Wallace* [1988].

4. Discussion and Conclusions

[11] When interpreting these results, it is important to remember that travel-time and attenuation measurements are laterally varying residuals with no depth constraints. Travel-time and attenuation anomalies at any location may represent separate anomalies at different depths. Nevertheless, our method isolates the sensitivity to upper-mantle structure beneath each station. While high- and low-velocity anomalies encountered along the same ray path can result in negligible travel-time residuals, high attenuation generally dominates over low attenuation resulting in high attenuation residuals.

[12] Seismic velocity variations are typically interpreted as anharmonic and anelastic variations due to temperature, composition, and physical state. While multiple sources, such as partial melt, strain, grain size, and composition can increase attenuation, water concentration and temperature likely have the largest effect on attenuation in the upper mantle [e.g., *Jackson et al.*, 1992, 2002; *Karato*, 2003]. Elevated temperatures cause high attenuation and slow seismic velocities. So, high mantle temperatures beneath the western US, inferred from the high surface heat flow, thin crust, and high elevation, are likely responsible for the high shear-wave attenuation and delayed arrivals observed there.

[13] Alternatively, subducted water associated with the Farallon slab may have elevated the mantle water content, which would result in increased anelasticity, effectively increasing attenuation and consequently decreasing seismic velocity. Ongoing subduction of the Juan de Fuca plate beneath the far northwest likely causes the observed high attenuation and delayed arrivals, as seen in other subduction zones [e.g., *Roth et al.*, 1999]. The low attenuation and slow velocities observed near Yellowstone and Cascadia are hard

to relate to thermal effects. Recent volcanism due to elevated temperature may have depleted the mantle of water in isolated regions, reducing present-day attenuation relative to the surrounding mantle [*Hammond and Humphreys*, 2000; *Humphreys et al.*, 2003b].

[14] The Precambrian mid-continental craton has fast seismic velocities, but normal to slightly elevated attenuation, which indicates that temperature alone cannot be responsible for the seismic anomaly [e.g., *Goes and van der Lee* [2002]. It is unlikely that the craton could maintain a distinct low temperature anomaly over the past $\sim$1 Ga. Chemical alteration within the deep root of the cratonic keel may increase seismic velocity [*Jordon*, 1979] without significantly altering attenuation. Moderately slow velocities and modest attenuation along the Atlantic Coast may indicate moderately high mantle temperatures [e.g., *Goes and van der Lee*, 2000]. The low surface heat flow anomaly beneath the Appalachians is accompanied by low attenuation and average to high seismic velocity, indicative of relatively cool mantle, having last modified more than 350 Ma.

[15] The Farallon slab is the most likely structure to cause bias to our attenuation measurements due to scattering. Small-scale scattering can cause energy loss that in some cases contaminates attenuation measurements. Focusing and defocusing can result in frequency dependent amplitude variations. However, we see little evidence for biases caused by the slab in our attenuation measurements. If a slab or other scattering object were responsible for the observed attenuation residuals, we would expect to see roughly north-south trending anomalies in western North America.

[16] While the cluster analysis approach works for large-scale variations, the method is increasingly effective for smaller, more densely populated networks due to increased waveform coherence. When applied to *P*- and *S*-waves measured at long-period seismic stations in North America, the attenuation structure is revealed. While some anomalies match expectations of thermal variations inferred from seismic velocity, other attenuation anomalies indicate other sources, requiring further investigation. Future application of this approach to the high station density of USArray may provide greater resolution and understanding of the North American continent.

[17] **Acknowledgments.** We thank two anonymous reviewers. The IRIS DMS provided the data. NSF grant EAR- EAR02-29323 funded this research.

References

Bassin, C., G. Laske, and G. Masters (2000), The current limits of resolution for surface wave tomography in North America, *Eos Trans AGU*, *81*(48), Fall Meet. Suppl., Abstract S12A-03.

Der, Z. A., and A. C. Lees (1985), Methodologies for estimating $t^*(f)$ from short-period body waves and regional variations of $t^*(f)$ in the United States, *Geophys. J. R. Astron. Soc.*, *82*, 125–140.

Durek, J. J., and G. Ekstrom (1996), A radial model of anelasticity consistent with long-period surface wave attenuation, *Bull. Seismol. Soc. Am.*, *86*, 144–158.

Flanagan, M. P., and D. A. Wiens (1994), Radial upper mantle attenuation structure of inactive back arc basins from differential shear wave measurements, *J. Geophys. Res.*, *99*, 15,469–15,485.

Goes, S., and S. van der Lee (2002), Thermal structure of the North American uppermost mantle inferred from seismic tomography, *J. Geophys. Res.*, *107*(B3), 2050, doi:10.1029/2000JB000049.

Hammond, W. C., and E. D. Humphreys (2000), Upper mantle seismic wave attenuation: Effects of realistic partial melt distribution, *J. Geophys. Res.*, *105*, 10,987–10,999.

Hartigan, J. A. (1975), *Clustering Algorithms*. John Wiley, Hoboken, N. J.

Humphreys, E., E. Hessler, K. Dueker, E. Erslev, G. L. Farmer, and T. Atwater (2003a), How Laramide-age hydration of North America by the Farallon slab controlled subsequent activity in the western U. S., in *The Lithosphere of Western North America and Its Geophysical Characterization: The George A. Thompson Volume, International Book Series*, vol. 7, edited by S. L. Klemperer and W. G. Ernst, pp. 524–544, Geol. Soc. Am., Boulder Colo.

Humphreys, E., E. Hessler, K. Dueker, G. L. Farmer, E. Erslev, and T. Atwater (2003b), How Laramide-age hydration of North American lithosphere by the Farallon slab controlled subsequent activity in the western United States, *Int. Geol. Rev.*, *45*, 575–595.

Jackson, I., M. S. Paterson, and J. D. Fitz Gerald (1992), Siesmic wave attenuation in Aheim dunite: An experimental study, *Geophys. J. Int.*, *108*, 517–534.

Jackson, I., J. D. Fitz Gerald, U. H. Faul, and B. H. Tan (2002), Grain-size-sensitive seismic wave attenuation in polycrystalline olivine, *J. Geophys. Res.*, *107*(B12), 2360, doi:10.1029/2001JB001225.

Jordan, T. H. (1979), Mineralogies, densities and seismic velocities of garnet, Lherzolites and their geophysical implications, *The Mantle Sample: Inclusions in Kimberlites and Other Volcanics Proceedings of the Second International Kimberlite Conference*, edited by F. R. Boyd and H. O. A. Meyer, pp. 1–14, AGU, Washington, D. C.

Kaben, M. K., and W. D. Mooney (2001), Density structure of the lithosphere in the southwestern United States and its tectonic significance, *J. Geophys. Res.*, *106*, 721–739.

Kane, M. F., and R. H. Godson (1989), A crust/mantle structural framework of the conterminous United States based on gravity and magnetic trends, in *Geophysical Framework of the Continental United States*, edited by L. D. Pakiser and W. D. Mooney, *Geol. Soc. Am. Mem.*, *172*, 383–403.

Karato, S.-I. (2003), Mapping water content in the upper mantle, in *Inside the Subduction Factory*, *Geophys. Monogr. Ser.*, vol. 138, edited by J. M. Eiler, pp. 135–152, AGU, Washington, D. C.

Lay, T., and D. V. Helmberger (1983), Body-wave amplitude and travel-time correlations across North America, *Bull. Seismol. Soc. Am.*, *73*, 1063–1076.

Lay, T., and T. C. Wallace (1988), Multiple ScS attenuation and travel times beneath western North America, *Bull. Seismol. Soc. Am.*, *78*, 2041.

Mooney, W. D., G. Laske, and T. G. Masters (1998), CRUST 5.1: A global crustal model at $5^\circ \times 5^\circ$, *J. Geophys. Res.*, *103*, 727–747.

Morgan, P., and W. D. Gosnold (1989), Heat flow and thermal regimes in the continental United States, in *Geophysical Framework of the Continental United States*, edited by L. D. Pakiser and W. D. Mooney, *Geol. Soc. Am. Mem.*, *172*, 493–522.

Patton, H. J., and S. R. Taylor (1984), Q structure of the Basin and Range from surface waves, *J. Geophys. Res.*, *89*, 6929–6940.

Pollack, H. N., S. J. Hurter, and J. R. Johnson (1993), Heat flow from the Earth's interior: Analysis of the global data set, *Rev. Geophys.*, *31*, 267–280.

Reif, C., G. Masters, P. Shearer, M. Flanagan, and G. Laske (2002), Cluster analysis of long-period waveforms: Implications for global tomography, *Eos Trans. AGU*, *83*(47), Fall Meet. Suppl., Abstract S51A-1017.

Roth, E. G., D. A. Wiens, L. M. Dorman, J. Hildebrand, and S. C. Webb (1999), Seismic attenuation tomography of the Tonga-Fiji region using phase pair methods, *J. Geophys. Res.*, *104*, 4795–4810.

Smith, W. H. F., and D. T. Sandwell (1997), Global sea floor topography from satellite altimetry and ship depth soundings, *Science*, *277*, 1956–1962.

Smith, W. H. F., and P. Wessel (1990), Gridding with continuous curvature splines in tension, *Geophysics*, *55*, 293–305.

van der Lee, S., and G. Nolet (1997), Upper mantle S velocity structure of North America, *J. Geophys. Res.*, *102*, 22,815–22,838.

VanDecar, J. C., and R. S. Crosson (1990), Determination of teleseismic relative phase arrival times using multi-channel cross correlation and least squares, *Bull. Seismol. Soc. Am.*, *80*, 150–169.

Venkataraman, A., A. A. Nyblade, and J. Ritsema (2004), Upper mantle Q and thermal structure beneath Tanzania, East Africa from teleseismic P wave spectra, *Geophys. Res. Lett.*, *31*, L15611, doi:10.1029/2004GL020351.

J. F. Lawrence, G. Masters, and P. M. Shearer, Institute of Geophysics and Planetary Physics, Scripps Institution of Oceanography, La Jolla, CA 92093–0225, USA. (jlawrence@ucsd.edu)